Analysis of signal dynamics in oxygen-enhanced magnetic resonance imaging

Olaf Dietrich, PhD[1]; Ulrike I. Attenberger, MD[2,3]; Michael Ingrisch, MSc[1]; Daniel Maxien, MD[2]; Michael Peller, PhD[1]; Konstantin Nikolaou, MD[2]; Maximilian F. Reiser, MD[1,2]

[1] Josef Lissner Laboratory for Biomedical Imaging, Department of Clinical Radiology – Grosshadern, LMU Ludwig Maximilian University of Munich, Munich, Germany

[2] Department of Clinical Radiology – Grosshadern, LMU Ludwig Maximilian University of Munich, Munich, Germany

[3] Institute of Clinical Radiology and Nuclear Medicine, University Hospital Mannheim, Medical Faculty Mannheim – University of Heidelberg, Mannheim, Germany

ELECTRONIC PREPRINT VERSION:
This is a non-final version of an article published in final form in Investigative Radiology.
Invest Radiol 2010; **45**(4): 165–173 <URL: http://dx.doi.org/10.1097/RLI.0b013e3181cd74e2>.

Abstract

Objectives: Oxygen-enhanced MRI (O2-MRI) is frequently based on a block paradigm consisting of a series of consecutive T1-weighted scans acquired during alternating blocks with inhalation of room air and of pure oxygen. This design results in a complex signal-time course for each pixel, which displays the oxygen wash-in and wash-out processes and provides spatially resolved information about the lung function. The purpose of the present study was to optimize the signal-time-course analysis in order to extract (pixelwise) the maximum amount of information from the acquired data, and to introduce an appropriate cross-correlation approach for data sets containing the oxygen wash-in and wash-out periods.

Materials and Methods: O2-MRI data of 11 healthy volunteers were acquired with a multislice inversion-recovery single-shot turbo-spin-echo sequence at 1.5 Tesla; lung and spleen were manually segmented on all 44 acquired slices. 6 different model functions were pixelwise fitted to the data and compared using the Akaike information criterion. 4 different reference functions were compared for cross-correlation analysis.

Results: The optimal model function is a piecewise exponential function (median enhancement in lung/spleen: 16.3 %/14.8 %) with different time constants for wash-in (29.4 s/72.7 s) and wash-out (25.1 s/29.6 s). As a new parameter, it contains the delay between switching the gas supply and the onset of the signal change (4.8 s/24.5 s). Optimal cross-correlation results were obtained with a piecewise exponential reference function, which was temporally shifted to maximize the correlation, yielding median correlation coefficients of 0.694 and 0.878, median time delays of 7.5 s and 38.6 s, and median fractions of oxygen-activated pixels of 83.6 % and 92.2 % in the lung and the spleen, respectively.

Conclusions: It was demonstrated that the pixelwise assessment of O2-MRI data is optimally performed with piecewise exponential functions. Cross-correlation analysis with a piecewise exponential reference function results in significantly higher fractions of oxygen-activated pixels than with rectangular functions.

Key words:
Oxygen-enhanced magnetic resonance imaging; Lung; Spleen; Oxygen wash-in/wash-out; Cross-correlation analysis

Corresponding author:
Olaf Dietrich, PhD
Josef Lissner Laboratory for Biomedical Imaging
Department of Clinical Radiology – Grosshadern
LMU Ludwig Maximilian University of Munich
Marchioninistr. 15
81377 Munich, Germany
Phone: +49 89 7095-3623, Fax: +49 89 7095-4627,
E-mail: od@dtrx.net

Introduction

Oxygen-enhanced MRI (O_2-MRI) has been successfully applied to visualize and assess pulmonary ventilation and lung function quantitatively or semi-quantitatively in several studies over recent years (1–21). The inhalation of pure oxygen (O_2), which acts as a weakly paramagnetic contrast agent, decreases the longitudinal relaxation time, T_1, of blood; the reduced relaxation time can then be detected as (a relatively small) signal enhancement in T_1-weighted MRI.

Frequently, a block paradigm is used to enhance the contrast-to-noise ratio of O_2-MRI consisting of a series of T_1-weighted scans acquired during alternating blocks with inhalation of room air and of 100 % O_2. This block design results in a signal-time course for each pixel containing information about lung function and about properties of respiration and circulation. Two different acquisition schemes for such block paradigms were used in past studies: (a) data acquisition can be paused for a few minutes after switching the gas supply to allow for establishing the new steady-state signal (2–6), or (b) T_1-weighted data can be acquired continuously, thus sampling the transition of the signal intensity towards the new steady-state value (7–14). An advantage of the first approach is that one has to deal only with static signal levels and that the signal difference between air and O_2 acquisitions (typically calculated after data averaging within each block) is maximized. It has been suggested to evaluate this time course by calculating the cross-correlation coefficient of each pixel response function and the (ideal) box-car waveform (3, 15). To quantitatively assess and compare the measured correlation coefficients in patients, the fraction of oxygen-activated pixels, f_{OAP}, has been defined as the fraction of lung pixels with correlation coefficients greater than 0.5 (5, 6).

In contrast, each pixel time course of the second approach contains the transitional signal that is observed immediately after switching the gas supply. These intermediary signal intensities reduce the averaged signal calculated within each block and, thus, decrease the observed mean signal enhancement. In order to optimize the signal enhancement maps, it has been suggested to discard some of the early transitional acquisitions to increase the observed signal enhancement (13). An advantage of the continuous data acquisition is that additional information about the O_2 wash-in and wash-out process can be obtained by analyzing the dynamic signal-time course. This was done before by either determining the linear slope of the signal change (8, 9) or by fitting an exponential function to the O_2 wash-in or wash-out data (7, 10, 12, 14). These studies demonstrated that, e. g., the slope correlates significantly with the pulmonary pathology (8, 9).

The purpose of the present study was to optimize the signal-time-course analysis in order to extract (pixelwise) the maximum amount of information from the continuously acquired data, and to introduce an appropriate cross-correlation approach for data sets containing the O_2 wash-in and wash-out periods. For the first aim, we evaluated and compared six reference functions modeling the complete O_2 wash-in and wash-out process with different numbers of fit parameters. Then, the optimal model function was used to establish reference values and the statistical distributions of the parameters in healthy volunteers. Finally, based on these results, we proposed and compared different reference functions for the cross-correlation analysis and determined the fraction of oxygen-activated pixels in O_2-MRI with continuous scanning.

Methods

We examined 11 non-smoking, healthy volunteers (7 male and 4 female) aged between 20 and 36 years; the volunteers gave written informed consent to participate in the study, which had local Ethics Committee approval.

All volunteers were imaged with a T_1-weighting multi-slice inversion-recovery half-Fourier-acquisition single-shot turbo-spin-echo (HASTE) sequence implemented on a 1.5-Tesla whole-body scanner (Magnetom Sonata, Siemens Healthcare, Erlangen, Germany) with a high-performance gradient system providing a maximum gradient strength of 40 mT/m and a maximum slope of 200 T/(m·s). An 8-channel phased-array thorax coil system was used for signal reception. An optimized inversion time, TI, of 1300 ms was chosen for T_1-weighting (15); images were acquired with linear k-space readout in phase-encoding direction (from left to right), a minimized echo time, TE, of 11 ms, and a receiver bandwidth of 795 Hz/pixel. The in-

plane image resolution was 3.1×3.1 mm² (matrix size 128×128, field of view 400×400 mm²); the generalized autocalibrating partially parallel acquisition (GRAPPA) technique was applied for parallel imaging with an acceleration factor of 2 (24 k-space lines were acquired in the k-space center immediately before the actual data acquisition to determine the GRAPPA reconstruction weights). The multi-slice sequence was based on an interleaved inversion and readout of 4 coronal slices (11) with a slice thickness of 8 mm and a slice distance of 16 mm. The data readout was both ECG and respiratory-triggered to ensure readout during end-expiration and in the diastolic phase; double-triggering has been suggested to optimize the image quality in O_2-MRI of the lung (6). The arms of the subjects were positioned above the head to minimize aliasing artifacts.

Each examination consisted of a series of 80 consecutive respiratory-gated acquisitions divided into 4 equally long blocks with alternating inhalation of room air and O_2 (20×air, 20×O_2, 20×air, 20×O_2). Thus, the total acquisition time was 80 respiratory cycles, i. e., it varied between about 8 and 12 minutes depending on the individual respiratory frequency, and the block duration of O_2 or air administration varied between about 2 and 3 minutes. The breathing gas was administered by a tightly fitting non-rebreathing respiratory face mask covering mouth and nose and with a gas flow of approximately 20 L/min.

Lung tissue and the spleen were segmented manually in all 11 data sets (44 slices). Then, bright vessels were automatically removed from the lung-tissue regions by defining the brightest 20 % of all lung-tissue pixels in each slice (maximum intensity projection over all repetitions) as vessels. Finally, image data were spatially smoothed by applying a Gaussian image filter with a size of 5×5 pixels and a width (standard deviation) of 2 pixels to all acquired slices.

The data post-processing and evaluation consisted of two separate parts. First, we searched for an optimal fitting function to the dynamic O_2-MRI data. In the second part, quantitative parameters determined with the optimal fitting function were used to establish an improved technique for cross-correlation analysis of dynamically acquired O_2-MRI data. All data post-processing (segmentation, smoothing, parameter fitting, and cross-correlation analysis) was performed with in-house developed dedicated software based on the free dynamic programming language Tcl/Tk.

For the first part of the evaluation, we restricted the data sets to the acquisitions #1 to #60, i. e., we discarded the last 20 acquisitions since these contained (in principle) the same dynamic data as acquisitions #21 to #40. By discarding these acquisitions, each data set consisted of 20 base line repetitions followed by 20 repetitions during O_2 wash-in followed by 20 repetitions during O_2 wash-out; thus, the subsequent analysis was based on an identical number of wash-in and wash-out acquisitions. Including acquisitions #61 to #80 as well would result in an over-representation of the wash-in process in the subsequent analysis, which might induce a bias in the derived results.

In order to reduce the remaining influence of respiratory motion, the diaphragm position was semi-automatically evaluated in all slices, and acquisitions with displaced liver-lung interfaces (of more than 1 pixel) were discarded.

We then normalized all data pixelwise to their mean value over the 20 initial baseline (air) acquisitions to obtain relative enhancement data. Only acquisitions #21 to #60 were used for the following analysis, in which we compared six different model functions, $f_m(t; p)$, $m = 1\ldots6$, for the evaluation of the signal-time course (see Fig. 1); here, t denotes the time point within the time course and p denotes the set of all other model parameters:

1. $f_1(t; p) = \mathrm{rect}(t;\ R_{enh}, \Delta t)$: a rectangular function (box-car waveform) with 2 free parameters (the relative enhancement, R_{enh}, and the time delay, Δt, between switching the gas supply and the onset of the signal change)
2. $f_2(t; p) = \mathrm{pw\_lin}(t;\ R_{enh}, \tau_{in}, \tau_{out}, \Delta t)$: a piecewise linear function with 4 free parameters (the relative enhancement, R_{enh}, the (normalized) wash-in up-slope, $1/\tau_{in}$, the (normalized) wash-out down-slope, $-1/\tau_{out}$, and the time delay, Δt)
3. $f_3(t; p) = \mathrm{pw\_exp}(t;\ R_{enh}, \tau_{in}, \tau_{out})$: a piecewise exponential function with 3 free parameters (the relative enhancement, R_{enh},

the wash-in time constant, τ_{in}, and the wash-out time constant, τ_{out})

4. $f_4(t; p)$ = pw_exp(t; R_{enh}, $\tau_{in/out}$, Δt): a piecewise exponential function with 3 free parameters (the relative enhancement, R_{enh}, only a single time constant, $\tau_{in/out}$, for wash-in and wash-out, and the time delay, Δt)
5. $f_5(t; p)$ = pw_exp(t; R_{enh}, τ_{in}, τ_{out}, Δt): a piecewise exponential function with 4 free parameters (the relative enhancement, R_{enh}, the wash-in time constant, τ_{in}, the wash-out time constant, τ_{out}, and the time delay, Δt)
6. $f_6(t; p)$ = pw_exp(t; R_{enh}, τ_{in}, τ_{out}, Δt, $\Delta t'$): a piecewise exponential function with 5 free parameters (the relative enhancement, R_{enh}, the wash-in time constant, τ_{in}, the wash-out time constant, τ_{out}, the time delay, Δt, describing the onset of the wash-in process, and the time delay, $\Delta t'$, describing the onset of the wash-out process).

The model functions were fitted pixelwise to the relative enhancement data using non-linear fitting with a box-constrained Levenberg-Marquardt implementation. The start value for fitting the relative enhancement, R_{enh}, was estimated as the mean relative enhancement over acquisitions #26 to #40; this parameter was constrained to the range from 0 to 100 %. The start value of the wash-in and wash-out time constants was set to 40 s for the exponential model functions and to the duration of the second room-air block divided by the start value of R_{enh} for the linear model function; in both cases, the parameters were constrained to the range from 0.5 s to 200 s. The start values of the time delays, Δt and $\Delta t'$, were set to 0 and constrained to the range from 0 to 100 s or 200 s for Δt and $\Delta t'$, respectively. A special procedure was required for the parameter fitting of the rectangular function, since the discontinuities of this function did not allow the direct application of the Levenberg-Marquardt algorithm. In this case, the optimal time delay, Δt, was determined as the time delay with the maximum correlation between the rectangular function and the signal-time curve; then, the optimal relative enhancement, R_{enh}, was fitted with the Levenberg-Marquardt algorithm.

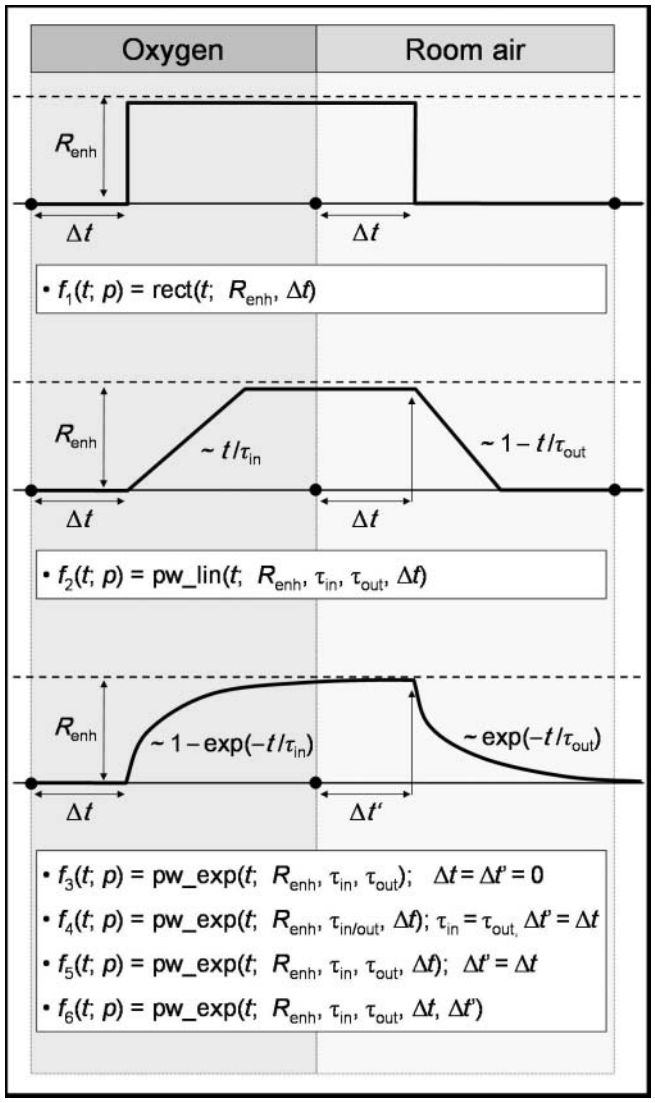

Figure 1: Six different model functions $f_m(t; p)$ with a set, p, of 2 to 5 free parameters (relative signal enhancement R_{enh}; time delays Δt, $\Delta t'$; wash-in and wash-out times τ_{in}, τ_{out}) for pixelwise fitting of O_2-MRI data; "rect": rectangular function, "pw_lin": piecewise linear function, "pw_exp": piecewise exponential function.

To assess the quality of the different fits, we first calculated for each pixel (with position **r**) and each model function the normalized sum of the squared differences, S_{sq}, between the fitted model functions, $f_m(t; p(\mathbf{r}))$, (the index m denotes the 6 different functions) and the original data points, $s(\mathbf{r}, t)$.

$$S_{sq}(\mathbf{r},m) = \frac{1}{N}\sum_{k=1\ldots N}\left(s(\mathbf{r},t_k) - f_m(t_k; p(\mathbf{r}))\right)^2$$

(the number, N, of data points could vary because of the motion correction). Then, the optimal fit function was determined using the corrected Akaike information criterion (cAIC), $C_{Akaike}(\mathbf{r}, m)$ (22), which is a measure based on the sum-of-squares difference, $S_{sq}(\mathbf{r}, m)$, the number, N, of

data points, and the number, K, of free fit parameters:

$$C_{\text{Akaike}}(\mathbf{r},m) = N\ln\left(S_{\text{sq}}(\mathbf{r},m)\right) + 2(K+1) + \frac{2(K+1)(K+2)}{N-K-2}$$

The optimal fit function is the one with the minimal cAIC. The probability that the model is the best among all considered models, i. e., that it approximates the data best without overfitting, is quantified by the Akaike weights (22):

$$w_{\text{Akaike}}(\mathbf{r},m) = \exp\left(-\Delta(\mathbf{r},m)/2\right) \Big/ \sum_{j=1}^{6} \exp\left(-\Delta(\mathbf{r},j)/2\right)$$

with $\Delta(\mathbf{r},m) = C_{\text{Akaike}}(\mathbf{r},m) - \min_{j=1\ldots6} C_{\text{Akaike}}(\mathbf{r},j)$. The median values of $C_{\text{Akaike}}(\mathbf{r}, m)$ and $w_{\text{Akaike}}(\mathbf{r}, m)$ were compared after averaging over all slices (lung without bright vessels and spleen) and all volunteers.

The model function with the lowest cAIC (or, equivalently, with the highest Akaike weight) was then used to calculate maps and averages (median value, 16th and 84th percentile) of all model parameters; parameters were evaluated separately for the spleen and the 4 different slices of the lung as well as for the total lung tissue.

The second main part of the data evaluation was focused on the application of cross-correlation approaches to dynamic O_2-MRI data. We defined four different reference functions, $r_m(t)$, $m = 1\ldots4$, to calculate the cross-correlation coefficients for each pixel time course: a rectangular box-car function, $r_1(t)$, as used in earlier publications (3, 5, 6, 15) and a piecewise exponential function, $r_2(t)$, similar to the optimal model function found in the first part of this study (see Fig. 2). The timing parameters for the piecewise exponential function were defined fixed as approximations to the median values over all lung pixels determined in the first part of this study. The cross-correlation coefficients, c_{CC}, defined as

$$c_{\text{CC}}(\mathbf{r},m) = \frac{\sum_k \left(s(\mathbf{r},t_k) - \overline{s(\mathbf{r},t_k)}\right)\left(r_m(t_k) - \overline{r_m(t_k)}\right)}{\sqrt{\sum_k \left(s(\mathbf{r},t_k) - \overline{s(\mathbf{r},t_k)}\right)^2}\sqrt{\sum_k \left(r_m(t_k) - \overline{r_m(t_k)}\right)^2}}$$

(the bar over a function denotes its mean value over all time points) were calculated for these two original functions and, additionally, for a set of time-shifted reference functions, $r_m(t; \Delta t_{CC})$, $m = 3,4$ (see Fig. 2). In the latter case, the correlation coefficients were calculated separately for 40 discrete time shifts, Δt_{CC}, by moving the first onset of the enhancement in the reference function from the 20th to the 21st … 60th acquisition within the time course. Then, the maximal correlation coefficient and the corresponding temporal shift, Δt_{CC}, over all shifted functions were pixelwise determined.

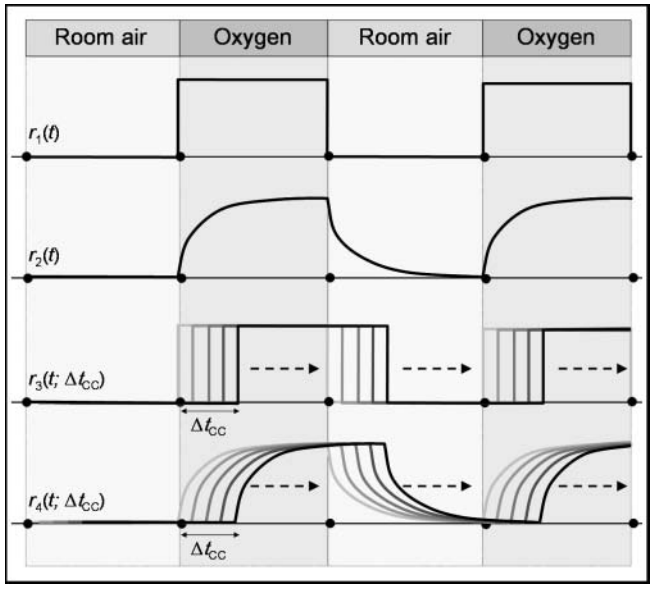

Figure 2: Four reference functions for cross-correlation analysis. $r_1(t)$: rectangular function (box-car waveform); $r_2(t)$: piecewise exponential function. The functions $r_{3,4}(t; \Delta t_{CC})$ are defined similar, but with an additional delay parameter, Δt_{CC}, that allows for temporal shifting of the function until maximum correlation is obtained.

We determined the median values, the 16th, and 84th percentile of the cross-correlation coefficients and of the temporal shifts evaluated over all segmented pixels (in all volunteers and all slices) for all four cross-correlation approaches. The fraction of oxygen-activated pixels, f_{OAP}, (i.e., with $c_{CC} > 0.5$) was calculated separately for each volunteer for the four used reference functions. The fractions of oxygen-activated pixels were then statistically compared with a paired Wilcoxon signed-ranks test.

Results

The segmented lung tissue in all 11 volunteers (over all 4 acquired slices) consisted of 89 539 pixels after removing the bright vessels; the segmented spleen tissue consisted of 8 836 pixels. The retrospective motion correction based on the diaphragm position resulted in an average acceptance

rate of 90.3 % (standard deviation: 15.0 %). The median values of the corrected Akaike information criterion and the Akaike weight evaluated over all pixels are listed in Table 1; an example of the regional distribution of the Akaike weights for all model functions is shown in Fig. 3. The model function with the minimal cAIC in lung tissue was the 3-parameter exponential model without delay parameter ($f_3(t; p)$ = pw_exp(t; R_{enh}, τ_1, τ_2), median of the cAIC: 135.4), closely followed by the 4-parameter exponential model ($f_5(t; p)$ = pw_exp(t; R_{enh}, τ_1, τ_2, Δt), median of the cAIC: 135.8). The model function with the minimal cAIC in spleen tissue was the 4-parameter exponential model ($f_5(t; p)$ = pw_exp(t; R_{enh}, τ_1, τ_2, Δt), median of the cAIC: 46.3). Thus, the 4-parameter exponential model, $f_5(t; p)$, was chosen for the subsequent quantitative analysis of O_2-MRI.

The median values of the fit parameters for $f_5(t; p)$ over all evaluated pixels are summarized in Table 2. Typical relative signal enhancements were between 15 % and 20 % with a moderate regional variance (16th to 84th percentile) between 8 % and 28 %. Typical time constants for O_2 wash-in and wash-out were between 25 s and 30 s; here, a larger regional variance was found with values ranging from 5 s to 80 s. There is no obvious position dependence of the parameters within the lung in anterior-posterior direction. Noteworthy are the substantial differences of the time delay, Δt, in the lung (Δt = 4.8 s) and the spleen (Δt = 24.5 s) as well as the prolonged wash-in time constant of 73 s in the spleen. Parameter maps of a volunteer are shown in Fig. 4 and (color-coded) in Fig. 1 of the Supplemental Digital Content.

Table 1: Median values of the corrected Akaike information criterion and the Akaike weight in all compared model functions

Model function	Corrected Akaike information criterion[a], C_{Akaike}			Akaike weight[b], w_{Akaike}		
	Lung tissue	Spleen tissue	Average of both	Lung tissue	Spleen tissue	Average of both
$f_1(t; p)$ = rect(t; R_{enh}, Δt)	146.2	86.4	116.3	0.014	< 0.001	0.007
$f_2(t; p)$ = pw_lin(t; R_{enh}, τ_{in}, τ_{out}, Δt)	137.5	48.3	92.9	0.094	0.148	0.121
$f_3(t; p)$ = pw_exp(t; R_{enh}, τ_{in}, τ_{out})	**135.4**	66.7	101.1	**0.251**	< 0.001	0.126
$f_4(t; p)$ = pw_exp(t; R_{enh}, $\tau_{in/out}$, Δt)	136.3	52.6	94.5	0.152	0.022	0.087
$f_5(t; p)$ = pw_exp(t; R_{enh}, τ_{in}, τ_{out}, Δt)	135.8	**46.3**	**91.1**	0.142	**0.151**	**0.147**
$f_6(t; p)$ = pw_exp(t; R_{enh}, τ_{in}, τ_{out}, Δt, $\Delta t'$)	138.2	47.5	92.9	0.039	0.105	0.072

[a] Minimal corrected Akaike information criterion is printed bold in each column.

[b] Maximal Akaike weight is printed bold in each column. Akaike weights do not sum to 1 since the median over all voxels (of an asymmetric distribution of weights) is displayed; for each single voxel, the sum of all weights is 1.

Table 2: Parameters of oxygen dynamics in healthy volunteers (median values, 16th…84th percentile), evaluated with $f_5(t; p)$

Region	R_{enh} (%)	τ_{in} (s)	τ_{out} (s)	Δt (s)
Lung slice 1 (anterior)	16.3 (7.6…30.4)	33.8 (2.1…96.1)	26.4 (0.5…92.5)	6.3 (0.0…25.2)
Lung slice 2	17.0 (9.2…29.9)	31.5 (3.4…84.1)	26.7 (5.8…71.3)	5.0 (0.0…25.3)
Lung slice 3	15.9 (9.4…25.9)	28.8 (8.5… 71.8)	25.4 (3.8…61.2)	6.5 (0.0…18.2)
Lung slice 4 (posterior)	16.3 (10.7…27.8)	27.3 (10.7…77.3)	23.3 (8.3…53.8)	0.9 (0.0…13.6)
Lung (all slices)	16.3 (9.5…28.1)	29.4 (6.9…79.4)	25.1 (5.4…64.8)	4.8 (0.0…18.9)
Spleen (all slices)	14.8 (8.1…20.6)	72.6 (44.4…184.6)	29.6 (14.3…50.5)	24.5 (13.6…41.8)

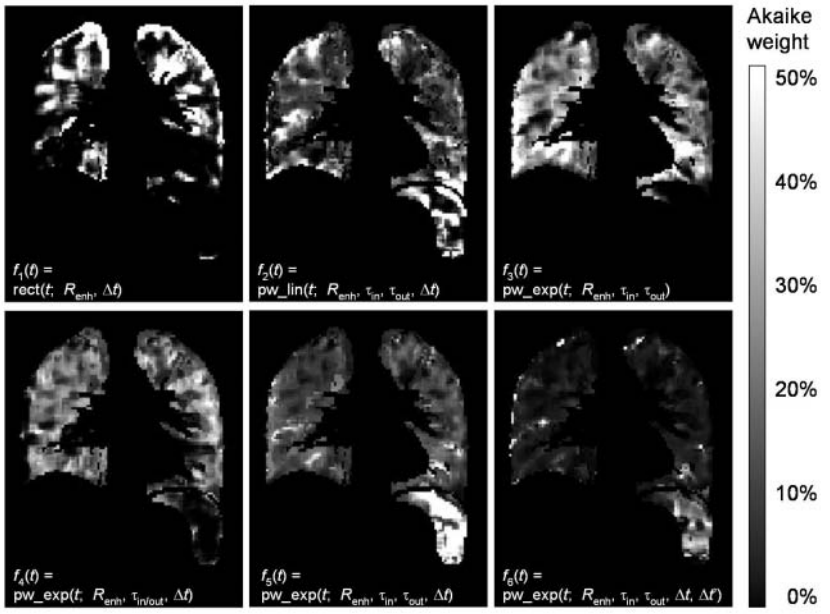

Figure 3: Parameter maps showing the regional distribution of the Akaike weights for the six compared model functions. The highest weights (indicating the best fit function) were obtained with f_3 in the lung and with f_5 in the spleen.

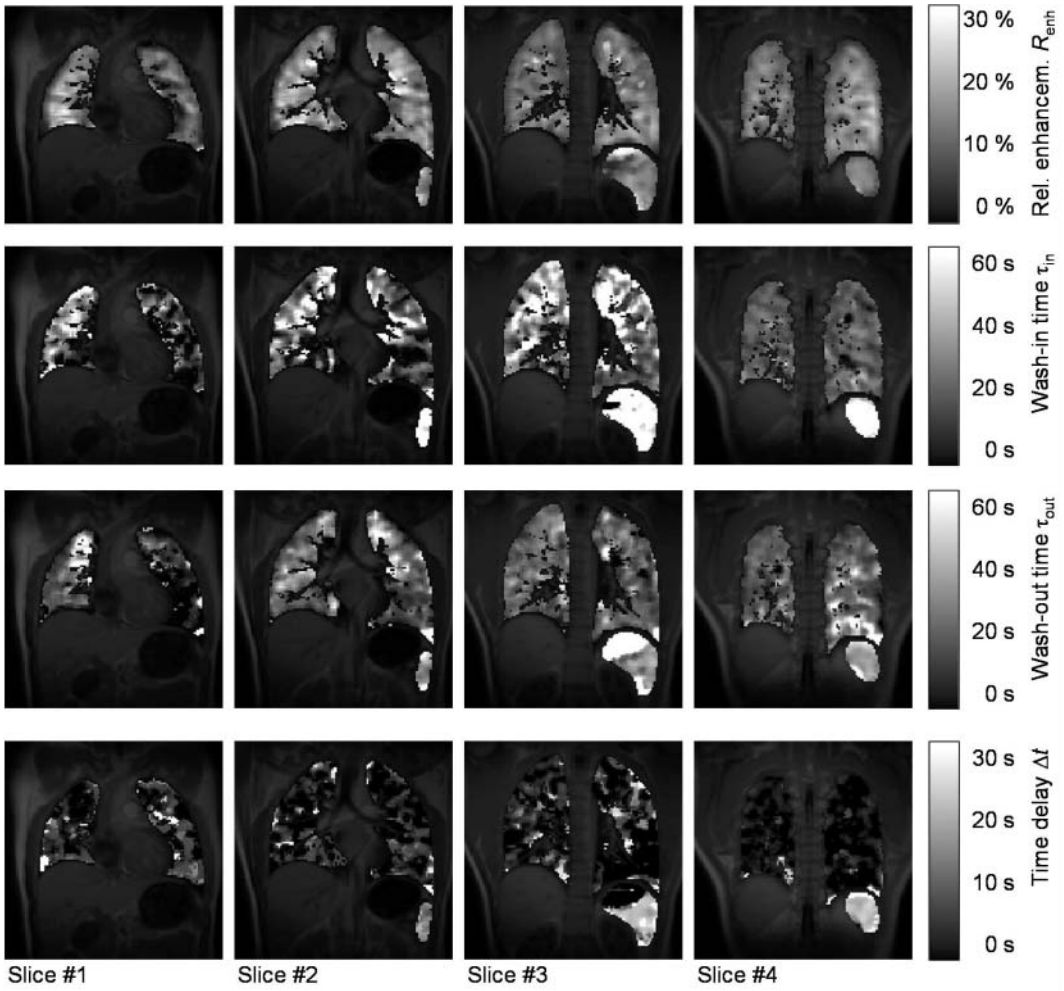

Figure 4: Parameter maps obtained by fitting the piecewise exponential 4-parameter model function, $f_5(t; p)$ = pw_exp(t; R_{enh}, τ_{in}, τ_{out}, Δt), to multislice O_2-MRI data from a healthy volunteer. 1st row: relative signal enhancement R_{enh}; 2nd row: O_2 wash-in time constant, τ_{in}; 3rd row: O_2 wash-out time constant τ_{out}; 4th row: time delay, Δt , between oxygen switching and the signal response. (The heterogeneous parameter distribution in the spleen is caused by partial volume effects of superposed stomach signal.). Color-coded maps of these results are provided as Fig. 1 of the Supplemental Digital Content (see below at the end of the manuscript).

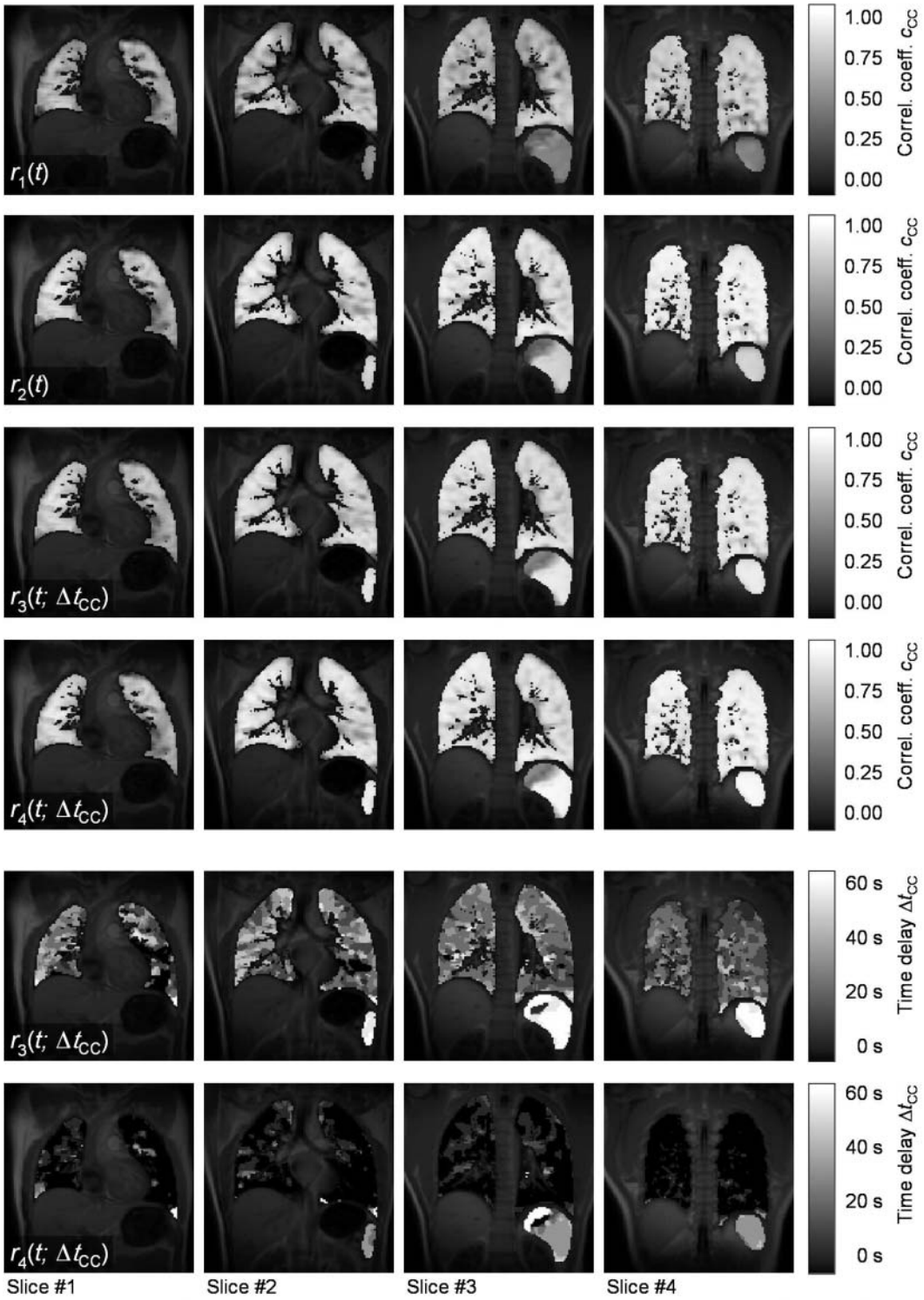

Figure 5: Parameter maps obtained by cross-correlation analysis of multislice O_2-MRI data from the same healthy volunteer as in Fig. 4. Rows 1 to 4 show the correlation coefficients (c_{CC}) of the signal-time course with different reference functions (rectangular wave, $r_1(t)$; piecewise exponential function, $r_2(t)$; rectangular wave shifted to obtain maximum correlation, $r_3(t; \Delta t_{CC})$; piecewise exponential function shifted to obtain maximum correlation, $r_4(t; \Delta t_{CC})$). Rows 5 and 6 show the delay, Δt_{CC}, with maximum correlation corresponding to rows 3 and 4. (The heterogeneous parameter distribution in the spleen is caused by partial volume effects of superposed stomach signal.) Color-coded maps of these results are provided as Fig. 2 of the Supplemental Digital Content (see below at the end of the manuscript).

Table 3: Comparison of cross-correlation results with different reference functions

Region	Reference function for cross-correlation; cf. Fig. 2		c_{CC}	Δt_{CC} (s)	f_{OAP} (%)
			median (16th…84th percentile) evaluation over all voxels		median over all volunteers
Lung	$r_1(t)$	rect.	0.470 (0.236…0.671)	–	39.5*
	$r_2(t)$	exp.	0.664 (0.387…0.847)	–	75.6†
	$r_3(t; \Delta t_{CC})$	rect.	0.668 (0.440…0.817)	31.0 (19.4…50.7)	83.0
	$r_4(t; \Delta t_{CC})$	exp.	0.694 (0.438…0.860)	7.5 (0.0…22.5)	83.6
Spleen	$r_1(t)$	rect.	0.341 (0.004…0.520)	–	0.2*
	$r_2(t)$	exp.	0.628 (0.344…0.822)	–	86.4†
	$r_3(t; \Delta t_{CC})$	rect.	0.823 (0.592…0.891)	64.9 (50.6…79.3)	92.5
	$r_4(t; \Delta t_{CC})$	exp.	0.878 (0.611…0.945)	38.6 (23.9…52.5)	92.2

* significantly lower (paired Wilcoxon signed-ranks test; $p < 0.01$) than with reference functions r_2, r_3, r_4

† significantly lower (paired Wilcoxon signed-ranks test; $p < 0.01$) than with reference functions r_3 and r_4

Based on the results in Table 2, we chose a wash-in time constant of 30 s and a wash-out time constant of 25 s for the exponential reference functions used for the cross-correlation analysis. The results of the compared cross-correlation approaches are presented in Table 3. The median values of the correlation coefficients over all pixels ranged from 0.34 with the fixed rectangular reference function to 0.88 with the shifted exponential function. Generally, the correlation coefficients depended more strongly on the reference function in the spleen than in the lung. The highest correlation coefficients were found with the shifted exponential function in both organs. The delay, Δt_{CC}, was about 7 s in the lung when evaluated with the exponential reference function; it was approximately 30 s longer in the spleen than in the lung with both reference functions. The delay was about 25 s longer with the rectangular than with the exponential reference function in both organs. Parameter maps are shown in Fig. 5 and (color-coded) in Fig. 2 of the Supplemental Digital Content.

The fractions of oxygen-activated pixels were significantly lower (p<0.01) with the fixed rectangular reference function than with all other functions. It was also significantly lower (p<0.01) with the fixed exponential function than with those two reference functions that were shifted to obtain the maximum correlation.

Discussion

In the present study, we provided a detailed analysis of the properties of the signal-time course in O_2-MRI by evaluating several model functions for the complete wash-in/wash-out process with different numbers of parameters. It was demonstrated that the experimental data are best fitted (evaluated by the corrected Akaike information criterion) by a piecewise exponential function with four free parameters: the relative signal enhancement, R_{enh}, the time constants of signal increase (O_2 wash-in) and decrease (O_2 wash-out), τ_{in} and τ_{out}, and the time delay, Δt, between switching the gas supply and the onset of the signal change. This result is in good agreement with the fact that the global O_2 concentration in the lung exhibits exponential time dependence after switching the O_2 concentration of the supplied gas (23). It furthermore indicates that the signal quality (in terms of temporal sampling rate and signal-to-noise ratio) is sufficient to reflect this exponential dependence; in the case of very low signal quality, the fit with the zeroth-order (rectangular) or first-order (linear) approximation of the exponential would be expected to show comparably good fit properties.

Reference values of these four parameters were established for our group of 11 non-smoking, healthy volunteers. The relative signal enhancement of about 16 % in the lung agrees well with earlier results by Müller et al. and Löffler et al. (9, 15), but were slightly lower than the enhancements

of 20 % to 25 % reported in some other studies (5, 14, 19, 20).

Pulmonary O_2 wash-in and wash-out times found in this study are in the range from 25 s to 30 s and agree well with results by Hatabu et al. (7), who also observed slightly longer wash-in than wash-out time constants. This difference has been explained in earlier studies as a consequence of pulmonary perfusion, which transports O_2 away from the lung and, thus, works towards wash-out and against wash-in (7, 10). Our time constants for O_2 wash-in agree well with those found in a study of preoperative oxygenation using end-tidal oxygraphy by Berry and Myles (24), although the authors state in their publication that the time for alveolar denitrogenation is subject to several factors such as the tidal volume and the ventilatory frequency. Comparing with other MR-based studies, our results lie between lower values of 17 s reported by Ohno et al. (14) and higher ones of about 45 s to 50 s found by Arnold et al. and Naish et al. (10, 12). Generally, these time constants are promising as indicators for several pulmonary pathologies such as emphysema, fibrosis, etc., which are known to cause an inhomogeneous dynamic distribution of inhaled gases (23); these inhomogeneities can now be depicted and quantified based on the maps of wash-in/out time constants.

In the spleen, the analysis of the O_2-induced signal changes has the advantage that the baseline tissue signal is substantially higher than in the lung and, thus, the signal-to-noise ratio of the dynamic signal-time course is higher as well. Hence, parameter fitting and the comparison of different model functions can be performed with higher reliability than in the lung tissue as indicated by the lower values of the Akaike information criterion. Our results show a similar relative signal enhancement in the spleen as in the lung, which is considerably lower than the values around 50 % reported by Tadamura et al. (25). This may be explained by the different inversion times used in both studies; the inversion time of 1300 ms used in the present study was optimized for lung tissue and may be too long for an optimal signal contrast in the spleen, which has a shorter T_1 time of about 800 ms to 1000 ms (25, 26). We found a substantially longer wash-in time (of about 70 s) in the spleen than in the lung reflecting the longer time required to reach a steady-state O_2 concentration in the blood and tissue outside the lung. Physiologically, one should differentiate between the time constants that describe the changing O_2 concentration in the alveolar volume, in the pulmonary capillaries, and in the tissue of other organs. While the O_2 concentration in the alveolar volume depends mainly on the respiratory parameters as mentioned above, longer time constants are observed in the blood pool and in particular in other organs because of the additional time required to reach a new steady-state O_2 concentration in tissue. Generally, this longer wash-in time (and its considerable regional variation with an 84th percentile of 185 s) should be taken into account in all studies (outside the lung) that rely on T_1-weighted signal changes after O_2 inhalation; we recommend an O_2 inhalation period of at least three times the wash-in time, i.e., of several minutes in order to obtain an optimal signal response. We are not aware of any other studies that report O_2 wash-in and wash-out time constants of the spleen.

A new parameter of our model function, which was not considered in former studies, is the time delay, Δt, that describes the interval between switching the gas supply and the onset of the signal change in the considered organ. This time delay is relatively short in lung tissue; the median value of about 5 s is in the range of single respiratory cycle. It is, however, substantially longer in the spleen (with a median of about 25 s) indicating perhaps the difference between O_2 accumulation in the pulmonary capillaries on the one hand and the change of O_2 concentration in the arterial blood pool as well as the circulation times to the spleen on the other hand. Further studies in patients with pulmonary diseases are required to investigate whether this new parameter can help in the characterization of diseased lung areas, which might be hypothesized to show a delayed onset (i.e. increased Δt) of O_2 enhancement due to locally restricted ventilation associated with a delay of local O_2 delivery. Outside of the lung, as e. g. in the spleen, Δt might correlate to the global lung function of patients, since delayed pulmonary oxygenation will induce related delays in all other organs as well; again, further patients studies are required to correlate the Δt in the spleen with any disease-related parameters.

We have demonstrated that the time-dependent relative signal enhancement in T_1-weighted O_2-MRI

is optimally fitted by a (piecewise) exponential model. It can be shown (cf. Appendix 1) that the observed behavior of the dynamic relative signal enhancement is in good approximation proportional to the time-dependent change of the O_2 concentration in blood or tissue. Thus, the calculated time constants (wash-in and wash-out times, τ_{in} and $\tau_{out,}$ as well as the delay, Δt) describe physiological tissue properties independent of the chosen measurement technique such as the pulse sequence or the sequence parameters. Hence, these quantitative results can be expected to be less examination-dependent than, e. g., the absolute or relative enhancement ratios or the slope of the signal changes.

Based on these results, we proposed and compared different approaches to analyze the cross-correlation properties and the fraction of oxygen-activated pixels in O_2-MRI with continuous scanning. We have shown that in dynamic O_2-MRI both the correlation coefficients and the fractions of oxygen-activated pixels depend significantly on the reference function used for cross-correlation analysis. With a box-car waveform as used in earlier studies (3, 5, 6, 15), the correlation parameters are substantially underestimated when the pixel time-course contains dynamic information from the O_2 wash-in and wash-out periods: e. g., by a factor of more than 2 in the spleen when comparing the (conventional) unshifted rectangular and the shifted exponential reference function. In the lung, the median correlation coefficient was below 0.5 with the conventional rectangular reference function; with all three other approaches it was between 0.65 and 0.70 in excellent agreement with Mai et al. (3). The optimal median correlation coefficient in the spleen was almost 0.9, which demonstrates the generally better signal-to-noise ratio in the spleen compared to the lung.

If the maximum correlation coefficient of a set of temporally shifted correlation functions is determined, then the temporal shift, Δt_{CC}, can be obtained as an additional parameter, which has a very similar interpretation as the time delay, Δt, determined by data fitting in the first part of our study and which might also be helpful, e. g., for the characterization of diseased lung areas in patients. If evaluated with the piecewise exponential function, Δt_{CC} is about 7.5 s in the lung and, thus, is comparable to the value of Δt of about 5 s. In the spleen, Δt_{CC} is about 39 s, which is somewhat longer than the corresponding value of Δt of about 25 s. This difference, however, may be explained by the longer O_2 wash-in time in the spleen that was not incorporated into the reference function (which was fixed for all pixels to the median values found in lung tissue); a longer delay increases the cross-correlation coefficient for spleen tissue by compensating the non-optimal shape of the reference function to a certain degree.

The observed difference of Δt_{CC} of about 25 s between correlation with the rectangular and the exponential reference functions agrees approximately with the shift of about 20 s that is required for a maximum correlation of the ideal rectangular and exponential functions.

The median fraction of oxygen-activated pixels depended strongly on the applied cross-correlation approach. It was below 50 % and, thereby, significantly lower with the fixed rectangular reference function used in earlier studies than with all other functions. With the time-shifted reference functions, we obtained fractions of oxygen-activated pixels of about 83 % in healthy volunteers, which agrees excellently with the result of 81.7 % reported by Molinari et al. (6). In the spleen, even higher fractions of oxygen-activated pixels (greater than 90 %) were found.

Generally, the cross-correlation techniques have the advantage that they are computationally less expensive than the non-linear fitting of a function with four free parameters; in addition, they are more robust in the presence of noise and of respiratory motion artifacts, both of which are typical for lung tissue in O_2-MRI. However, the full information content of the acquired data including the time constants for O_2 wash-in and wash-out can only be retrieved by the non-linear fitting procedure. A certain limitation of both techniques is that exact timing information of each acquired image is required for the analysis, since the respiratory triggering results in non-equidistant timing of the individual acquisitions. This timing information had to be extracted from the archived data sets prior to the subsequent image post-processing steps.

In conclusion, we provided a detailed analysis of the properties of the pixelwise evaluated signal-time course in O_2-MRI of the lung and the spleen demonstrating that the experimental data are best fitted by a piecewise exponential function. As a new parameter, the time delay between switching the gas supply and the onset of the signal change was introduced. We could also demonstrate that cross-correlation techniques can be significantly improved for the application in oxygen-enhanced MRI data acquired continuously over the O_2 wash-in and wash-out periods. Evaluating the full signal-time course either by model fitting or by cross-correlation allows extracting more information from the acquired data than in previous studies.

Appendix

In this Appendix we show that the observed behavior of the (T_1-weighted) dynamic relative signal enhancement, $\Delta S(t)/S_{air}$, is in good approximation proportional to the time-dependent change of the O_2 concentration, $\Delta c_{O2}(t)$, in the pulmonary blood or tissue.

The longitudinal relaxation rate, R_1, of lung tissue depends linearly on the O_2 concentration, c_{O2}, in the lung tissue including O_2 physically solved in blood, or (once a steady state is reached) on the O_2 concentration, $c_{O2,gas}$, in the breathing gas (21):

$$R_1 = R_{1,0} + r_1 \cdot c_{O2} = R_{1,0} + f_{OT} \cdot c_{O2,gas}$$

with the relaxation rate without oxygen, $R_{1,0}$, the relaxivity of molecular oxygen, r_1, and the effective oxygen-transfer function, f_{OT}. In the following, we define the oxygen-transfer function, f_{OT}, for O_2 concentrations ranging from 0 to 1 (and not to 100 %), i. e., a typical value for a healthy volunteer is $f_{OT} \approx 0.1\ s^{-1}$ (21). The description based on the oxygen-transfer function has the advantage that the concentration of the O_2 concentration in the breathing gas is much better accessible than the actual O_2 concentration in the tissue.

The dependence of the signal on the O_2 concentration seen with a T_1-weighting inversion-recovery experiment with inversion time, TI, is

$$\begin{aligned} S(c_{O2}) &= S_0\,[1 - 2\exp(-TI \cdot R_1(c_{O2}))] \\ &= S_0\,[1 - 2\exp(-TI \cdot (R_{1,0} + r_1 \cdot c_{O2}))] \\ &= S_0 - 2\,S_0 \exp(-TI \cdot R_{1,0})\exp(-TI \cdot r_1 \cdot c_{O2})), \end{aligned}$$

where S_0 denotes the fully relaxed signal. This expression can be approximated by linearizing the last exponential (using $\exp(-x) \approx 1 - x$ for sufficiently small x), since the exponent, $TI \cdot r_1 \cdot c_{O2} = TI \cdot f_{OT} \cdot c_{O2,gas} \approx 1.3\ s \cdot 0.1\ s^{-1} \cdot c_{O2,gas} = 0.13 \cdot c_{O2,gas}$ (with $c_{O2,gas}$ ranging from 0.21 to 1) is considerably lower than 1:

$$\begin{aligned} &S(c_{O2}) \approx \\ &S_0 - 2\,S_0 \exp(-TI \cdot R_{1,0})\,(1 - TI \cdot r_1 \cdot c_{O2}). \end{aligned}$$

Thus, the signal difference between two measurements with different O_2 concentrations, $c_{O2}^{(1)}$ and $c_{O2}^{(2)}$, is

$$\begin{aligned} &S\left(c_{O2}^{(2)}\right) - S\left(c_{O2}^{(1)}\right) \approx \\ &2 \cdot S_0 \cdot \exp\left(-TI \cdot R_{1,0}\right) \cdot TI \cdot r_1 \cdot \left(c_{O2}^{(2)} - c_{O2}^{(1)}\right), \end{aligned}$$

which is proportional to the change of the O_2 concentration, $\Delta c_{O2} = c_{O2}^{(2)} - c_{O2}^{(1)}$. The relative signal enhancement with respect to the signal during the inhalation of room air, which was determined in the present study, is therefore also proportional to the change of the O_2 concentration,

$$\begin{aligned} \frac{\Delta S(c_{O2}(t))}{S\left(c_{O2}^{(air)}\right)} &= \frac{S(c_{O2}(t)) - S\left(c_{O2}^{(air)}\right)}{S\left(c_{O2}^{(air)}\right)} \approx \\ &\frac{2 \cdot S_0 \cdot \exp\left(-TI \cdot R_{1,0}\right) \cdot TI \cdot r_1}{S\left(c_{O2}^{(air)}\right)} \cdot \Delta c_{O2}, \end{aligned}$$

and, thus, the quantitative evaluation of the relative signal enhancement reflects the properties of the actual O_2 concentration in lung tissue.

References:

1. Edelman RR, Hatabu H, Tadamura E, et al. Noninvasive assessment of regional ventilation in the human lung using oxygen-enhanced magnetic resonance imaging. Nat Med. 1996;2:1236–1239.
2. Müller CJ, Löffler R, Deimling M, et al. MR lung imaging at 0.2 T with T1-weighted true FISP: native and oxygen-enhanced. J Magn Reson Imaging. 2001;14:164–168.
3. Mai VM, Tutton S, Prasad PV, et al. Computing oxygen-enhanced ventilation maps using correlation analysis. Magn Reson Med. 2003;49:591–594.
4. Ohno Y, Hatabu H, Higashino T, et al. Oxygen-enhanced MR imaging: correlation with postsurgical lung function in patients with lung cancer. Radiology. 2005;236:704–711.
5. Molinari F, Gaudino S, Fink C, et al. Simultaneous cardiac and respiratory synchronization in oxygen-enhanced magnetic resonance imaging of the lung using a pneumotachograph for respiratory monitoring. Invest Radiol. 2006;41:476–485.
6. Molinari F, Eichinger M, Risse F, et al. Navigator-triggered oxygen-enhanced MRI with simultaneous cardiac and respiratory synchronization for the assessment of interstitial lung disease. J Magn Reson Imaging. 2007;26:1523–1529.
7. Hatabu H, Tadamura E, Chen Q, et al. Pulmonary ventilation: dynamic MRI with inhalation of molecular oxygen. Eur J Radiol. 2001;37:172–178.

8. Ohno Y, Hatabu H, Takenaka D, et al. Oxygen-enhanced MR ventilation imaging of the lung: preliminary clinical experience in 25 subjects. AJR Am J Roentgenol. 2001;177:185–194.

9. Müller CJ, Schwaiblmair M, Scheidler J, et al. Pulmonary diffusing capacity: assessment with oxygen-enhanced lung MR imaging preliminary findings. Radiology. 2002;222:499–506.

10. Arnold JF, Fidler F, Wang T, et al. Imaging lung function using rapid dynamic acquisition of T1-maps during oxygen enhancement. MAGMA Magn Reson Mater Phy. 2004;16:246–253.

11. Dietrich O, Losert C, Attenberger U, et al. Fast oxygen-enhanced multislice imaging of the lung using parallel acquisition techniques. Magn Reson Med. 2005;53:1317–1325.

12. Naish JH, Parker GJ, Beatty PC, et al. Improved quantitative dynamic regional oxygen-enhanced pulmonary imaging using image registration. Magn Reson Med. 2005;54:464–469.

13. Dietrich O, Losert C, Attenberger U, et al. Oxygen-enhanced MRI of the lung: optimized calculation of difference images. Radiologe. 2006;46:300–308.

14. Ohno Y, Koyama H, Nogami M, et al. Dynamic oxygen-enhanced MRI versus quantitative CT: pulmonary functional loss assessment and clinical stage classification of smoking-related COPD. AJR Am J Roentgenol. 2008;190:W93–W99.

15. Löffler R, Müller CJ, Peller M, Penz et al. Optimization and evaluation of the signal intensity change in multisection oxygen-enhanced MR lung imaging. Magn Reson Med. 2000;43:860–866.

16. Ley S, Puderbach M, Risse F, et al. Impact of oxygen inhalation on the pulmonary circulation: assessment by magnetic resonance (MR)-perfusion and MR-flow measurements. Invest Radiol. 2007;42:283–290.

17. Boss A, Schaefer S, Martirosian P, et al. Magnetic resonance imaging of lung tissue: influence of body positioning, breathing and oxygen inhalation on signal decay using multi-echo gradient-echo sequences. Invest Radiol. 2008;43:433–438.

18. Molinari F, Puderbach M, Eichinger M, et al. Oxygen-enhanced magnetic resonance imaging: influence of different gas delivery methods on the T1-changes of the lungs. Invest Radiol. 2008;43:427–432.

19. Mai VM, Chen Q, Bankier AA, et al. Multiple inversion recovery MR subtraction imaging of human ventilation from inhalation of room air and pure oxygen. Magn Reson Med. 2000;43:913–916.

20. Mai VM, Bankier AA, Prasad PV, et al. MR ventilation-perfusion imaging of human lung using oxygen-enhanced and arterial spin labeling techniques. J Magn Reson Imaging. 2001;14:574–579.

21. Jakob PM, Wang T, Schultz G, et al. Assessment of human pulmonary function using oxygen-enhanced T(1) imaging in patients with cystic fibrosis. Magn Reson Med. 2004;51:1009–1016.

22. Glatting G, Kletting P, Reske SN, et al. Choosing the optimal fit function: comparison of the Akaike information criterion and the F-test. Med Phys. 2007;34:4285–4292.

23. Comroe JH, Forster RE, Dubois AB, et al. The lung; clinical physiology and pulmonary function tests. Chicago, IL: Year Book Medical Publishers; 1962.

24. Berry CB, Myles PS. Preoxygenation in healthy volunteers: a graph of oxygen "washin" using end-tidal oxygraphy. Br J Anaesth. 1994;72:116–118.

25. Tadamura E, Hatabu H, Li W, et al. Effect of oxygen inhalation on relaxation times in various tissues. J Magn Reson Imaging. 1997;7:220–225.

26. O'Connor JP, Naish JH, Jackson A, et al. Comparison of normal tissue R1 and R*2 modulation by oxygen and carbogen. Magn Reson Med. 2009;61:75–83.

Supplemental Digital Content

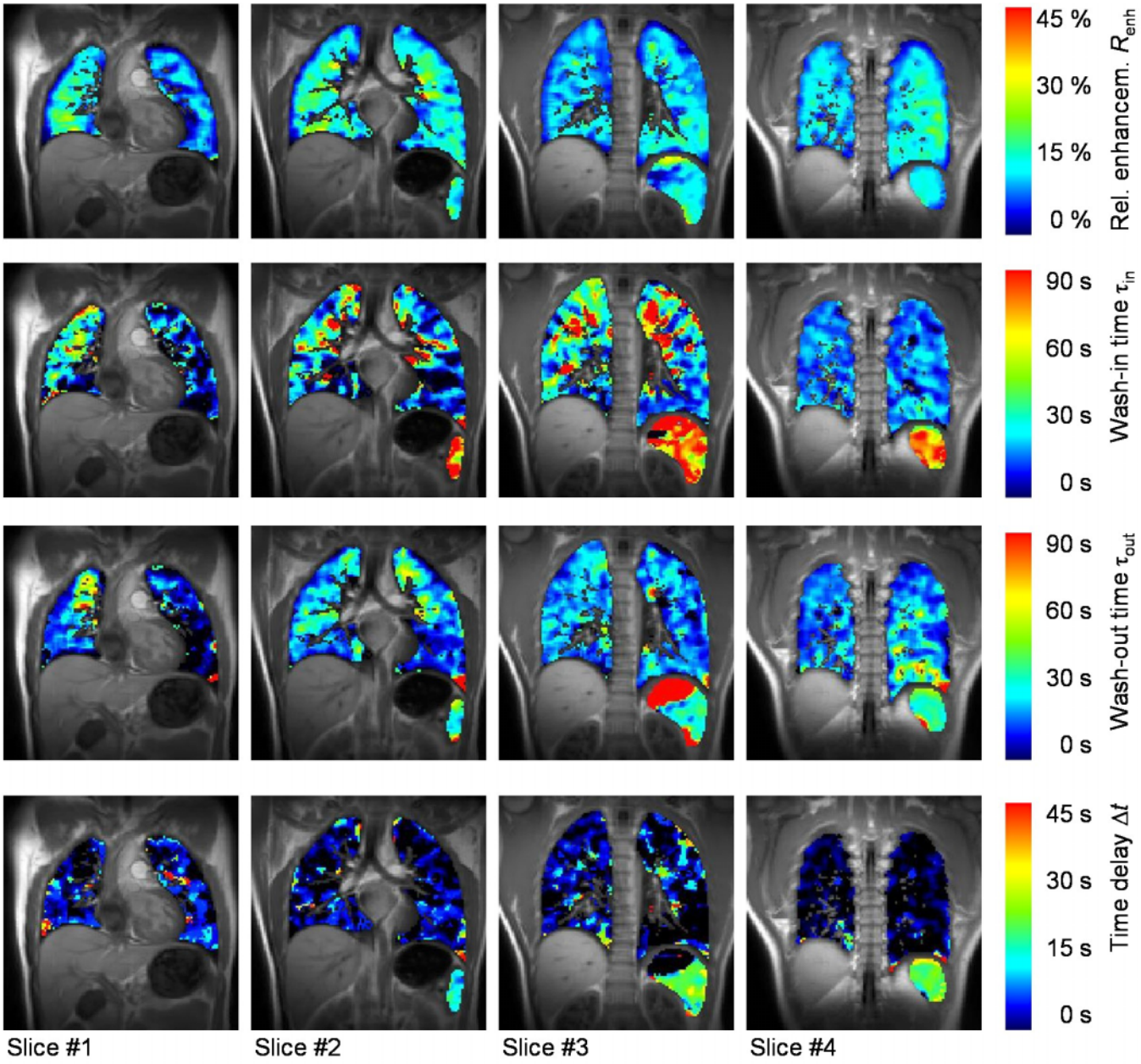

Figure 1 of the Supplemental Digital Content (cf. Fig. 4 above)

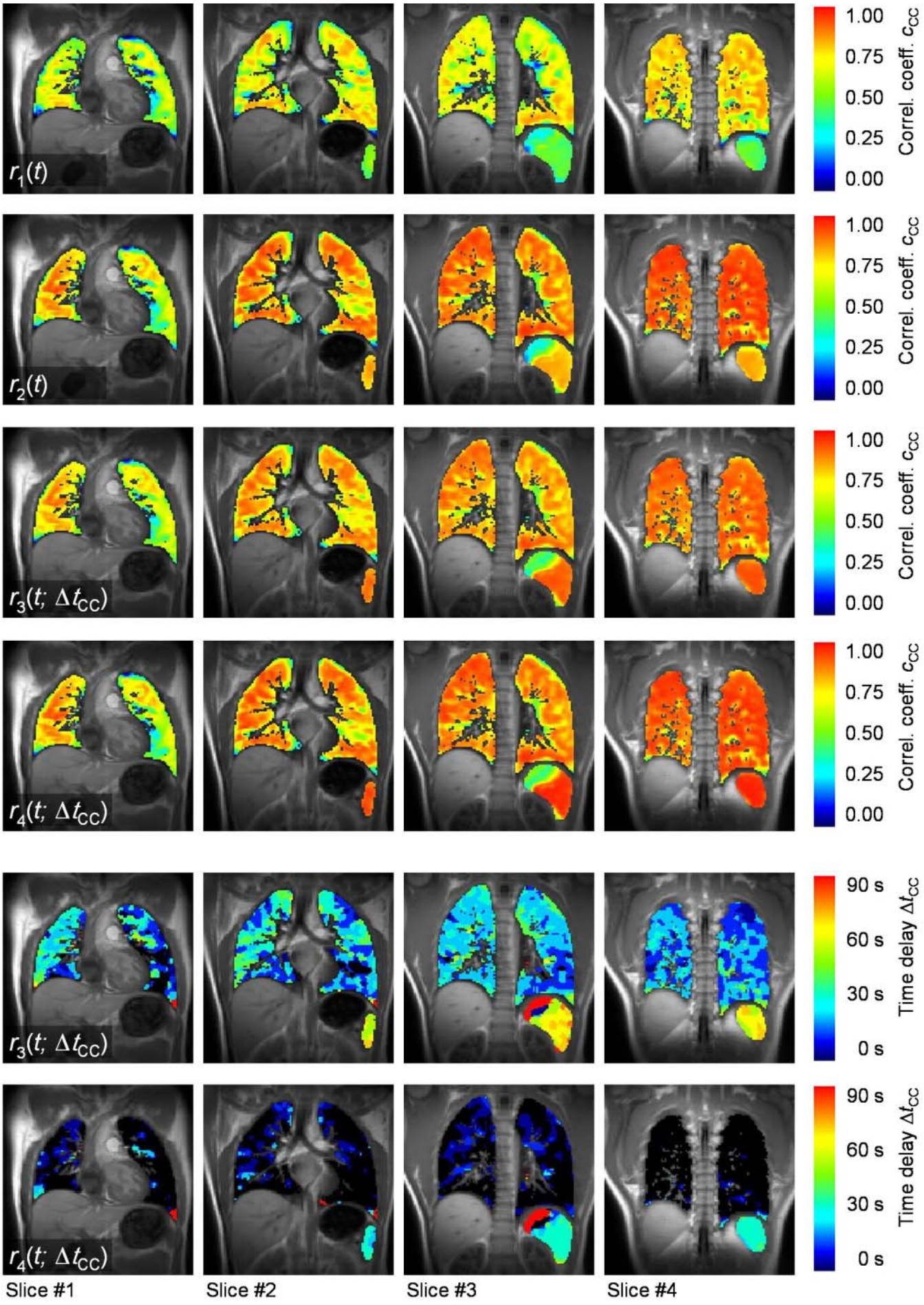

Figure 2 of the Supplemental Digital Content (cf. Fig. 5 above)